RSC Advances

ROYAL SOCIETY OF CHEMISTRY

www.rsc.org/advances

Synthesis, characterization and cytotoxicity of europium incorporated ZnO-graphene nanocomposites on human MCF7 breast cancer cells

Susanta Bera[1], Monisankar Ghosh[2#], Moumita Pal[1#], Nilanjana Das[1], Suchandrima Saha[2], Samir Kumar Dutta[2] and Sunirmal Jana[*1] ([#]Authors contributed equally to this work)

[1]Sol-Gel Division, CSIR-Central Glass and Ceramic Research Institute,
196 Raja S.C. Mullick Road, P.O. Jadavpur University, West Bengal, Kolkata 700032, India.

[2]Drug Development Diagnostic & Biotechnology, CSIR-Indian Institute of Chemical Biology,
4 Raja SC Mullick Road, P.O. Jadavpur University, West Bengal, Kolkata 700032, India.

Abstract

Europium incorporated ZnO-chemically converted graphene (CCG) nanocomposites (ZEG) were synthesized by adopting solvothermal process at 95^{o}C from the precursors of varying europium nitrate to zinc acetate molar ratio (R = 0.00, 0.05, 0.10, 0.15) in a fixed content of graphene oxide. Eu level (R value) in the precursors found to play a role on tailoring the crystallite / particle size of hexagonal ZnO as evidenced from X-ray diffraction / transmission electron microscopy analysis. Existence of chemical interaction / complexation between the oxygen functionalities of CCG and inorganic moieties (ZnO/Zn^{2+} and Eu ions) of nanocomposites was studied by FTIR, Raman, UV-Vis spectral and XPS measurements. The nanocomposites possessed meso pores as confirmed from BET nitrogen adsorption isotherm and the sample ZEG(10) (R = 0.10) found to possess the highest specific surface area. In spite of an UV emission at ~385 nm, an orange emission (appeared at 595 nm) along with other visible emissions was also observed from the photoluminescence spectra of nanocomposites. However, intensity of the orange emission (λ_{ex} = 400 nm) found maximum in ZEG(10) sample

which produced relatively bright orange fluorescence images of human breast cancer cells (MCF7) under confocal laser scanning microscope. This could indicate the internalization of the nanomaterials within the cells. As obtained from MTT assay, the samples ($R \geq 0.10$) exhibited comparatively low in-vitro cytotoxicity (higher cell viability) on the cancer cells. The low cytotoxicity could be explained on the basis of I_D/I_G (intensities of D and G bands of graphene) value of CCG as realized from Raman spectral measurement. The nanocomposite ZEG(10), owning relatively large surface area, bright cell imaging capability and better cell viability, could be employed for cancer cell targeted optical imaging and drug delivery.

Key words: Solvothermal synthesis, Eu incorporation, nano ZnO, chemically converted graphene, photoluminescence, cell imaging and cytotoxicity

*****Corresponding author: Tel.: +91 33 23223303, fax: +91 33 2473 0957
E-mail: sjana@cgcri.res.in, janasunirmal@hotmail.com (S. Jana)

Introduction

Now-a-days, graphene based nanocomposites (NCs) have sparked a greater attention to the materials scientists in both basic and applied fields of research.[1-3] Although, graphene is a 2-dimensional (2D) monolayer sheet of in-plane sp^2 bonded carbons having unaffected p_z orbitals, however, research community[4,5] commonly called all its family members (e.g. graphene oxide, GO; chemically converted graphene (CCG) / reduced graphene oxide, rGO) as "graphene" and in fact, the members could able to form functional NCs with polymers (e.g. polyaniline, polyvinyl alcohol),[6,7] metal/ metal ions (e.g. Ag, Au, Pt/ Eu ion)[8-11] and metal oxides (e.g. ZnO, TiO_2, Fe_3O_4, MnO_2, SnO_2, Co_3O_4).[12-17] Thus, in the NCs, an advancement of properties[6,18] (such as electrical, optical, electrochemical and mechanical) could be achieved. This would find enormous applications[6,13,14,19-22] (e.g. cellular imaging, bacterial toxicity, drug delivery, enzyme sensing, photothermal therapy, photocatalytic, Li-ion batteries, supercapacitors, photovoltaic devices) of the NCs.

ZnO is well known functional semiconductor oxide[23-26] having wide direct band gap (3.37 eV, at room temperature) and large exciton binding energy (60 meV). Owning to characteristic UV emission, it could be an important material for optoelectronic application.[25] Moreover, several visible emissions[26] could be observed under a single light excitation due to formation of surface defects in ZnO. All these emissions could also be tuned through doping / controlling the parameters during materials synthesis.[23-29] Alternatively, the optical property of the semiconductor could also be modified[12] through the formation of nanocomposite with graphene. In a basic aspect of nanocomposite, Son *et al.*[12] reported that Zn^{2+} ions chemisorbed on the embryo of ZnO nanoparticles which could react with the oxygen functional groups of GO,

leading to the formation of Zn-O-C bonding. In addition, the GO sheets could be exfoliated chemically in the reaction medium. On the other hand, graphene is more biocompatible[30] because the living cell could well adhere and proliferate on graphene sheets[31]. However, the nanoparticles are generally toxic in nature but the toxicity of the nanoparticles could be mitigated to make the material biocompatible and nontoxic[20] through their proper surface modification with graphene. It could also be noted[12,32] that the exfoliated graphene when rich in oxygen containing functional groups (carboxylic, hydroxyl and epoxide) could interact with suitable cations (adsorbed on the semiconductor oxide surface),[12] resulting the formation of graphene based functional nanocomposites. However, the functional groups could interact with cations and would help to generate reactive sites towards the nucleation and crystal growth of nanoparticles.[32] But in the nanocomposites, the GO could transform into chemically converted graphene (CCG) (also called reduced graphene oxide, rGO) with lesser number[33] of oxygen containing functional groups. Sometimes, the highly toxic nanoparticles (for example, CdSe/ZnS quantum dots) could tag[20] with rGO and would make them potential biomaterials for applications of in-situ monitored bright fluorescence imaging and photothermal therapy of living cells. On the other hand, the presence of large numbers of oxygen functional groups in GO would create more toxic effect on living cells compare to CCG/rGO.[34] This would be caused due to chemical interactions[34] between the functional groups of GO and living cells. In fact, the living cells when combine with GO enhances mitochondrial respiration rate by donating its available electrons and creates reactive oxygen species (ROS).[34] Although, ZnO is known to be a biocompatible[24] material but due to the particle dissolution[35] in tissue culture medium, it could show toxic effects on living cells. During the particle dissolution, Zn^{2+} ions shedding could damage lysosomes, perturbs mitochondria, generates ROS, etc. In this context,

by Fe doping, the dissolution could be reduced though the changes of particle matrix as the dopant could easily be entered into the ZnO lattice.[35]

In europium graphene composite, europium shows higher adsorption energy with lower diffusion barrier compare to other rare earths[11]**.** Moreover, europium ions could form complexes with oxygen functional groups of graphene that could be revealed by FTIR, Raman spectral and XPS measurements. In addition, the graphitic carbons could quench[11,36] the fluorescence of organic dyes. Wang et al[36] synthesized three dimensional europium-complexed rGO macroassembly by one-pot self-assembly process. The authors reported the formation of inner-sphere surface complexes of europium ions and confirmed the formation of Eu(II) ions by XPS analysis and claimed that the reduction of Eu(III) to Eu(II) ions took place due to complexation.[36,37] Although, several authors[38-40] already reported Eu incorporated ZnO nanoparticles but a very few of them claimed[38] that the Eu enters into the crystal lattice. The problem of incorporation could be addressed due to the large size of europium ions compare to Zn^{2+}.[40] However, it was already been reported that depending upon the incorporation level[41] of rare earths, an increase of surface defects were found in ZnO as assessed from photoluminescence emission spectral study. [26,41]

Generally, the synthesis of graphene based nanocomposites could mostly be done by solvothermal,[21,25] chemical deposition[42] and microwave-assisted[43] processes. However, the low temperature solvothermal process could be advantageous over others. Recently, many exciting properties were observed in graphene based ternary nanocomposites (e.g. Fe_3O_4-graphene-TiO_2, rGO-porphyrin-ZnO, graphene-Fe_2O_3-polyaniline and Pt-ITO-graphene).[44-47] The composite materials could be used in photoconversion, photovoltaics, supercapacitors etc. However, to the best our knowledge, no report was found on Eu incorporated ZnO-graphene (ZEG)

nanocomposites which would generate a new class of ternary nanocomposite materials for emerging applications. Thus, on the aspects of both basic and applied fields of research, the synthesis of graphene-based ZEG nanocomposites would be very promising.

In the present work, a systematic study was performed on the synthesis of europium incorporated ZnO-chemically converted graphene (CCG) nanocomposites (ZEG) from the precursors of varying europium nitrate to zinc acetate molar ratio (R = 0.00, 0.05, 0.10, 0.15) in a fixed content of graphene oxide by adopting a low temperature (95^{o}C) solvothermal process. In the nanocomposites, the influence of Eu incorporation level (in terms of R value) on crystallite/particle size of hexagonal ZnO, existence of chemical interaction/complexation and optical properties were analyzed. Moreover, the cell imaging capability of the samples was studied under confocal laser scanning microscope. Finally, in-vitro cell viability in terms of cytotoxicity of the nanocomposites on MCF7 breast cancer cells from MTT assay was also verified.

Experimentals

Synthesis of graphene oxide (GO)

Graphene oxide (GO) was prepared (see **electronic supporting information** for details) from graphite powder following modified Hummer's method.

Synthesis of Eu incorporated ZnO-chemically converted graphene (ZEG) nanocomposites

We adopted a facile low temperature (95^{o}C) solvothermal process for the synthesis of europium incorporated ZnO-chemically converted graphene (ZEG) nanocomposites using as-synthesized graphene oxide (GO), zinc acetate dihydrate ($Zn(CH_3COO)_2.2H_2O$, ZA, Sigma-Aldrich, ≥98%)

and europium nitrate pentahydrate ($Eu(NO_3)_3.5H_2O$, EUN, Sigma-Aldrich, 99.9%) in dimethyl formamide (DMF, a polar aprotic solvent) medium. Four different nanocomposites were prepared by varying EUN / ZA molar ratio (R); 0.00, 0.05, 0.10 and 0.15 in the precursors and these were designated as ZEG(00), ZEG(05), ZEG(10) and ZEG(15), respectively. All the samples were prepared separately and in each preparation, a fixed amount (60 mg) of as-synthesized GO was uniformly dispersed in DMF (40 ml) by ultrasonication for about 60 min duration. Further, the GO dispersed in DMF was mixed with a definite quantity of ZA (0.95 g) and the requisite amount of EUN while stirring continuously to form stable precursors for ZEG nanocomposites. Subsequently, the precursors were kept in an air oven at 95^{o}C up to 9 h (maximum) following X-ray diffraction results (**Fig. S1, electronic supporting information**). After heating, the colour of the mixtures found to change from black to grayish white that signified the formation of ZEG nanocomposites. The solid materials as dispersed phase were then separated out by centrifugation. In each preparation, the product was re-dispersed in ethanol and then in double distilled water followed by centrifugation for isolation from the dispersion medium. Finally, the samples were dried in an air oven at ~55^{o}C. It was noteworthy to mention that the reduction of GO could be achieved via thermal annealing (>1000^{o}C), photochemical reduction and electrochemical reduction processes.[33] However, in the present work, none of the processes was adopted. Hence, we called the GO in the nanocomposites as chemically converted graphene (CCG).

Characterizations

Materials characterization

X-ray diffraction (XRD) study of the samples was performed by employing an X-ray diffractometer (Bruker D8 Advance with DAVINCI design X-ray diffraction unit) with nickel-filtered CuK_α radiation source (λ =1.5418 Å) in the 2θ range, 5^o – 80^o. Transmission electron microscopy / high resolution transmission electron microscopy (TEM/HRTEM) along with TEM-EDS measurements on the samples were performed by FEI Company make (Tecnai G^2 30.S-Twin, Netherlands) machine at the accelerating voltage of 300 kV. Carbon coated 300 mesh Cu grids were used for placement of the samples. For the measurements, the samples were dispersed in methanol by ultrasonication and the dispersed nanocomposites were placed on the Cu-grid carefully. Moreover, to identify the layers of chemically converted graphene (CCG) onto the nano ZnO crystals in ZEG(00), the TEM measurements were also performed by using a JEOL JEM-2100F (FEG) high-resolution electron microscope operated at an accelerating voltage of 200 kV. FTIR spectral study was carried out by Thermo Electron Corporation, USA make FTIR spectrometer (Nicolet 5700). For each experiment, the number of scans was fixed at 100 (wavenumber resolution, 4 cm^{-1}). Absorption spectra of the samples were recorded by diffused reflectance method using an UV-VIS-NIR spectrophotometer (UV3600, Shimadzu, Japan) with ISR 3600 attachment. Raman spectra were measured using micro-Raman (Renishaw inVia Raman microscope). An argon ion laser with an incident wavelength of 514 nm was used as the excitation source. X-ray photoelectron spectrum (XPS) in the range of 200 – 1200 eV of a representative sample, ZEG(10) was carried out to determine chemical state and chemical interaction/complexation of elements present in the sample by employing PHI Versaprobe II Scanning XPS microprobe surface analysis system using Al-K_α X-rays (hν,

1486.6 eV; ΔE, 0.7 eV at room temperature). The pressure in the XPS analysis chamber was better than $5x10^{-10}$ mbar. The energy scale of the spectrometer was calibrated with pure (Ag) sample. The position of C1s peak was taken as standard (binding energy, 284.5 eV). Room temperature photoluminescence (emissions and excitations) spectral property of the samples was measured by Perkin-Elmer (LS55) spectrofluorimeter. The slit widths for the measurements of emissions and excitations spectra were kept fixed at 2.5 nm and 10 nm, respectively for all the samples. In each sample, a pellet with approximately 0.5 mm was prepared for the PL and PLE measurements. The surface area, pore size and pore volume of the nanocomposites were measured by nitrogen adsorption and desorption studies at liquid nitrogen temperature by adopting a Quantachrome (Autosorb1) machine. All the samples were out gassed in the vacuum at suitable temperature for about 4 h prior to measurement.

Cytotoxicity and cell imaging studies

Cytotoxicity measurement of three representative nanocomposites (ZEG(00), ZEG(10) and ZEG(15)) on human cell line MCF7 (breast cancer cell, procured from National Centre for Cell Science, Pune, India) were performed. We used Dulbecco's modified eagles medium (DMEM, St. Louis, Missouri, USA), fetal bovine serum (FBS, Carlsbad, CA, USA), PenStrep (Life Technologies, Carlsbad, CA, USA) and MTT (3-[4,5-dimethylthiazol-2-yl]-2,5-diphenyltetrazoliumbromide, Carlsbad, CA, USA) as necessary chemicals and reagents.

Cell culture

The MCF7 cells were cultured in DMEM (invitrogen) supplemented with 10% fetal bovine serum (FBS) and antibiotic (1% penicillin/streptomycin) in 5% CO_2 at 37^{o}C. The cells from exponentially growing cultures were used for the experiments.

Measurement of in vitro cellular cytotoxicity, MTT assay

The MTT assay was done to estimate the viable cells. In brief, MCF7 cells (10^4 cells per well) were seeded on to a flat bottom 96-well plate and incubated at 37^{o}C in 5% CO_2. Cells were treated with or without (i.e. vehicle control) nanocomposite at their varying concentrations, ranging from 5 to 200 µg/ml and kept for 24 h. Finally, it was subjected to MTT assay. Then, 20 µl of MTT (5 mg/ml) was added to each well. After four hours of incubation, the media was removed and cells were dispersed in 200 µl of dimethyl sulphoxide (DMSO) solvent. Absorbance spectra of the samples were measured at 595 nm wavelength by Thermo MULTISKAN EX plate reader (Thermo, USA). The cell viability values were expressed in percentages with respect to control values.

Confocal Laser Scanning Microscopy (CLSM) study

Cell internalization of two representative nanocomposites (ZEG(00) and ZEG(10)) was visualized under confocal laser scanning microscopy (CLSM) at 405 nm laser source. The MCF7 cells were cultured to enough confluent on a cover slide at 37^{o}C in 5% CO_2. Then, the cells were separately treated with individual nanocomposite (concentration, 100 µg/ml) as well as vehicle control (without nanocomposite) for 2 h. Finally, the cells were thoroughly washed twice by PBS and visualized under the Andor Spinning Disc Confocal Microscope at 20x magnification and the images were captured using Andor IQ2 software.

Results and discussion

Figure 1 displays the XRD patterns of ZEG nanocomposites and as-synthesized graphene oxide (GO). The XRD pattern of GO shows[48] a strong diffraction (2θ) peak at 10.9^{o} (interlayer spacing, 8.12 Å) along (002) plane in addition to a weak peak at 42.4^{o} for (100) plane. However, the XRD peaks of GO found to disappear gradually on increasing reaction time and after 9 h, the peaks were not seen (**Fig. S1, electronic supporting information**) from the synthesis of ZEG(00) nanocomposite. This could suggest a complete conversion of GO to chemically converted graphene (CCG) took place in the nanocomposite. However, no obvious peaks[48] of CCG were found that might be due[49] to interaction/complexation between the organic and inorganic moieties of the nanocomposite (discussed later). On the other hand, the formation of hexagonal ZnO (**Fig. S1, electronic supporting information**) was observed at least in 7 h reaction time but an appreciable intensity of XRD peaks for the oxide was found in 9 h. Therefore, we fixed the reaction time at 9 h for the synthesis of Eu incorporated ZEG nanocomposites. In ZEG samples, the observed XRD peaks were fully matched with hexagonal ZnO (h-ZnO) [JCPDS 36-1451] and no additional diffraction peaks corresponding to europium oxide[38] was found. Moreover, in the Eu incorporated samples, the XRD peak shifting compare to ZEG(00) was not visualized. In fact, there was a little possibility of Eu incorporation in nano h-ZnO crystal lattice through substitution of Zn site by Eu. This would be due[39,40] to larger ionic radius of europium ions (Eu^{3+}, 0.95 Å or Eu^{2+}, 1.17 Å)[50] compare to zinc ions (Zn^{2+}, 0.74 Å).[26] Moreover, the small crystallite size might create an unfavorable condition that would lead to hinder incorporation of Eu into nano ZnO crystal.[26] We also calculated the crystallite size of h-ZnO from the XRD patterns at (101) plane using Scherrer's equation.[26] On increasing Eu incorporation level, it was found that the crystallite size (**inset, Fig. 1**) increased with an

exception in ZEG(10) where lower size of ZnO in the nano regime was obtained compare to ZEG(05) and ZEG(15). As Eu was neither entered into the ZnO crystal lattice nor formed any europium oxide; hence, it was hopefully existed as complexed (discussed later) species with the organic moiety (CCG) of the nanocomposites. In this context, very recently, Pal et al[26] observed that an excess dopant would remain onto the ZnO crystal surface and suppressed its grain growth at higher doping level in Al doped nanostructured ZnO thin films by sol-gel process. In the present work, the probability of Eu ions to be present directly onto the crystal surface might not valid because we found an increase of crystallite size in the nanocomposite, ZEG(15) having higher level of Eu than ZEG(05) and ZEG(10). Thus, the matter of Eu incorporation into the ZnO-CCG composite would create a new structure. In the later discussion, we find out a possible chemical structure of ZEG nanocomposites. However, the reason for attaining relatively low crystallite size in ZEG(10) compare to ZEG(05) and ZEG(15) was not clear to us and we would open this issue for the future.

TEM results of nanocomposites are given in **Figure 2 and Figure S2, electronic supporting information**. From the TEM images (**Fig. 2a, c, e; Fig. S2**), the agglomeration of composite nanoparticles seemed to be diminishing at the higher level of Eu incorporation and anyhow, nearly monodispersed quasi spherical particles (**Fig. 2e**) were resulted in ZEG(15). However, on increasing Eu level, the trend in change of average size of the particles obtained from the histograms (**insets, Fig. 2 c, e; Fig. S2 a, b**), constructed from their respective TEM images found identical with the calculated crystallite size (**inset, Fig. 1**) of h-ZnO as obtained the XRD patterns. Moreover, the particle size obtained from TEM analysis found always higher than the calculated value from XRD patterns. This difference could suggest the formation of ZEG nanocomposite particles because the calculated crystallite size from XRD considered only

for h-ZnO but the observed nanoparticles in TEM images could be for the nanomaterials consisting of inorganic (ZnO/Zn^{2+} and Eu ion) and organic (CCG) moieties (discussed later). In HRTEM images (**Fig. 2b, d, f**) of the nanocomposites, the lattice fringe with regular spacing of 0.26 nm is fully consistent[12] with the interplanar distance of (002) plane of h-ZnO. Although, the XRD patterns of nanocomposites did not evidence the presence of CCG but their corresponding TEM images clearly shows a sheet-like structure (**Fig. 2**) which could be originated from CCG layers. This sheet-like structure was the CCG layers present in the nanocomposites as also evidenced from its fast Fourier transform (FFT) patterns (**inset (ii) of Figure 2(e)**). The FFT shows a set of spots corresponding to crystallographic planes, (002) and (101) of h-ZnO along with (002) of CCG. In addition, as seen from the HRTEM image (**Fig. 2b**) of ZEG(00), the layers of chemically converted graphene (CCG) sheets of nearly ~3 nm thickness onto the nano ZnO crystals is clearly visible. Thus, the CCG layers could make Eu incorporated ZnO@CCG core-shell-like structure in the nanocomposite. Irrespective of incorporation level, it was not possible to quantify the Eu content from the TEM-EDS (insets, Fig. 2d,f) analysis of ZEG nanocomposites. This was because the characteristic peaks in EDS of Eu could be disguised[39] within the broad peaks of Zn and Cu.

The presence of chemical interaction / complexation between the oxygen functionalities of CCG with inorganic moieties (ZnO/Zn^{2+} and Eu ions) was verified by FTIR vibrational spectra. **Figure 3** and **Figure S3** represent the FTIR spectra of ZEG nanocomposites and as-synthesized GO**.** In GO, the presence[33] of hydroxylates, carboxylates and epoxides in the form of oxygen functional groups, C-OH, C–O–C, O-H (deformation) and –COOH were distinctly observed from the appearance of vibrations located at ~1070 cm^{-1}, ~1225 cm^{-1}, ~1400 cm^{-1} and ~1735 cm^{-1}, respectively.[11,21,51] In addition, a skeletal vibration of unoxidized graphitic domains

in GO was also found at ~1620 cm^{-1}. [51] However, the intensity of all the vibrational peaks found to decrease to a large extent in the GO derived nanocomposites (ZEG(00), ZEG(10) and Eu-CCG). In addition, a new vibration observed at ~1570 cm^{-1} in ZEG(00), ZEG(10) and Eu-CCG samples assigned to the characteristic skeletal vibrations of graphitic domains of CCG.[21] This result could favour the conversion of GO to chemically converted graphene (CCG) in the nanocomposites[33] and corroborated the TEM result (**Fig. 2**). However, the complete conversion of GO to CCG was found at least in 9 h of reaction time which could easily be understood from the FTIR spectral study (**Fig. S3, electronic supporting information**) of the representative (ZEG(00)) nanocomposites, synthesized by changing reaction times. In addition, a strong vibration appeared at 1375 cm^{-1} in Eu-CCG could be ascribed to the symmetric stretching vibration due to complexation of –COOH group with europium ions[36,52] (Eu^{3+}/Eu^{2+}) (discussed later under XPS result, **Fig. 5**). Moreover, its asymmetric stretching component[52] might be overlapped within the broad vibration (~1570 cm^{-1}) of graphitic domains of CCG. Perhaps, the asymmetric and symmetric stretching vibrations[53] of complexed –COOH groups of CCG with Zn^{2+} remained as ZnO/Zn^{2+} (discussed later) would disguise within the broad spectral vibrations of the graphitic domains and the spectral region, 1470-1320 cm^{-1}, respectively. However, the FTIR spectra of both ZEG(00) and ZEG(10) nanocomposites showed a strong vibration at ~460 cm^{-1} which was not observed in europium-CCG nanocomposite (Eu-CCG), assigned[21,54] to Zn-O bond vibration. Moreover, a sharp vibration appeared at 418 cm^{-1} in Eu-CCG that might be overlapped within the broad vibration region of Zn-O in ZEG(10), attributed to Eu-O bond vibration.[36]

Raman spectra of ZEG nanocomposites are displayed in **Figure 4**. The Raman peaks located at 325 cm^{-1}, 434 cm^{-1}, 571 cm^{-1} and ~1135 cm^{-1} ascribed to[21-25] the modes of $2E_2$(M),

E_2(high), E_1(LO) and $2E_1$(LO) of hexagonal wurtzite ZnO respectively. In fact, the E_2(high) mode could be recognized as the signature of h-ZnO that was already confirmed by XRD (**Fig. 1**) and TEM (**Fig. 2**) studies. In addition, the defect band, D (intensity I_D) at ~1350 cm^{-1} as a breathing mode of k-point phonons in A_{1g} symmetry, appeared in all the nanocomposites including precursor GO.[12,25] This could strongly suggest the existence of defects in the graphene moiety.[25,49] In GO, the Raman peak observed at 1597 cm^{-1} was assigned to E_{2g} phonon of sp^2 carbon atoms[12,25] and designated as graphene (G) band (intensity I_G). However, the G band found to shift in the ZEG nanocomposites by 14±2 cm^{-1} towards lower energy region[11,25] with respect to the band in GO while the location of the D band remained approximately at the same position. Moreover, a systematic broadening[11] of the D band was observed on increasing Eu level. The peak broadening could assess from the calculation of half width at full maxima (FWHM) (**Table S1, electronic supporting information**) of the peak at 1350 cm^{-1}. These results obviously supported the conversion of GO to CCG, existed as chemically interacted/ complexed with inorganic moieties (ZnO/Zn^{2+} and Eu^{3+}/Eu^{2+} ions) during the synthesis process. It could be noted that the chemical interaction / formation of complexes were also noticed from the FTIR vibrational spectra (**Fig. 3; Fig. S3, electronic supporting information**) of the ZEG nanocomposites. On the other hand, on increasing Eu level, a systematic enhancement of the intensity ratio, I_D/I_G was found (**Fig. 4, Table S1 of electronic supporting information**) up to R = 0.10 (ZEG(10)) that remained same in the next higher incorporation level in ZEG(15). The D band could be associated[11] with the complexed oxygen functionalities of CCG. Moreover, the relative increase of the D band intensity could also be accounted for the exfoliation[46] of graphene layers that could be possible via chemical interaction / complexation with the inorganic moieties of nanocomposites. Therefore, on increasing Eu level in a fixed amount of

CCG, the complexed oxygen functionalities in ZEG nanocomposites could expect to reach a value with an optimum concentration of europium (Eu^{3+}/Eu^{2+}) ions. As no evidence of Eu oxide formation which could support the incorporation of Eu into ZnO crystal lattice was found in the XRD patterns (**Fig. 1**), and thus, the europium ions should remain in the complexed species with CCG of the nanocomposites. Hence, no further change in the content of free oxygen functionalities might be available after the Eu incorporation level ($R \geq 0.10$), and consequently, a fixed value of I_D/I_G was found. Although, we explained the possible interaction / complex formation between the inorganic moieties and the oxygen functionalities in the nanocomposites but the existence of $Zn^{2+}$and Eu^{2+}/Eu^{3+} could not be ascertained by the Raman spectral study.

XPS analysis could also be a useful tool[11,21,38] to confirm the interaction of oxygen functionalities of CCG with the inorganic moieties. Thus, the XPS measurement (**Fig. 5**) of a representative sample, ZEG(10) was performed to confirm the chemical state/(s) of the elements as well as the chemical interactions existing between the organics, CCG and the inorganic moieties ((ZnO/Zn^{2+} and Eu^{3+}/Eu^{2+} ions) of the nanocomposite. The XPS survey spectrum (**Fig. S4, electronic supporting information**) shows the binding energy signals for C1s, O1s, Zn2p and Eu3d core levels. A broad signal for C1s could be resolved (**Fig. 5a**) into three Gaussian peaks centered at 284.4 eV (a1), 285.4 eV (a2) and 288.8 eV (a3) which correspond to Sp^2C, Sp^3C and O-C-O respectively[22,36] from the organic moiety, CCG in the sample. The O1s peak (**Fig. 5b**) could also be decomposed into three distinct components with binding energies ~530.1 eV (S1), 531.8 eV (S2) and 533.1 eV (S3). The S1 signal could be due to the lattice oxygen (O^{2-})[26] of hexagonal ZnO whereas the higher binding energy signals of O1s (S2, S3) could associate with the presence of chemically interacted / complexed oxygen functional groups (epoxy/COOH/hydroxyl)[36] of CCG. On the other hand, the strong binding energy signals

located (**Fig. 5c**) at 1044.3 eV and 1021.6 eV assigned to $Zn2p_{1/2}$ and $Zn2p_{3/2}$ core levels,[21] respectively. In this work, we observed a shifting (~2 eV) of the Zn2p signals towards higher energy compare to pure ZnO as already reported by Zhang *et al.*[21] This result could imply the presence of interaction and electron transformation between ZnO/Zn^{2+} moiety and oxygen functionalities of CCG.[21] However, an energy difference of 22.7 eV between the binding energy levels found well supported for the existence of Zn^{2+} in the nanocomposite.[26] Although, the XRD (**Fig. 1**) and TEM (**Fig. 2**) studies could not evidence the presence of Eu, but the XPS (**Figure 5d**) confirmed the core level binding energies of Eu3d. The intense doublets appeared at 1164.6 eV and 1134.7 eV could be assigned to the energy levels of $Eu3d_{3/2}$ and $Eu3d_{5/2}$, respectively in Eu^{3+} species.[36,38] In addition, the existence of Eu^{2+} species were also evidenced from relatively weak binding energy signals located at 1155.4 eV and 1124.4 eV of Eu^{2+} $3d_{3/2}$ and Eu^{2+} $3d_{5/2}$ components, respectively.[36] In this synthesis, the presence of Eu^{2+} could be originated from the reduction of Eu^{3+} in CCG environment.[36] Mercier *et al.*[55] reported a $M_mX_xO_y$ type oxo-compound which shows a higher core level binding energy compare to M_aO_b. Here, M (M = Eu) is more electropositive element than X (X = C) and consequently, the M-O bond is more ionic character than X-O bond. In X-O-M bond, the electrons could pull away from M and the Eu^{2+} formed as a result of diminishing the valency of Eu^{3+}. Therefore, both Eu^{2+} and Eu^{3+} ions could associate with the free oxygen functional groups of CCG and would form $M_mX_xO_y$ type complex in the nanocomposites. Thus, it could expect that at the higher Eu incorporation level, it would reduce the free oxygen functional groups of CCG. This would help to minimize the toxicity (discussed later, **Fig. 9b**) of nanocomposites on living cells because the oxygen functionalities could easily be interacted with the cells.[34]

In **Figure 6,** UV-Vis absorption spectral (measured by diffused reflectance method) results of GO and ZEG nanocomposites are given. Appearance of two prominent absorption peaks at 232 nm and ~290 nm (broad shoulder, **inset (i), Fig. 6**) in GO could correspond to $\pi \rightarrow \pi^*$ and $n \rightarrow \pi^*$ transitions of C=C and C=O bands,[56] respectively. However, in all the nanocomposites, the peak at 232 nm found red-shifted to ~270 nm while the peak at ~290 nm noticed to disappear completely in the Eu incorporated nanocomposites. This result could signify[56] that a strong coupling exists between the inorganic moieties (ZnO/Zn^{2+} and Eu^{3+}/Eu^{2+} ions) and the CCG during the conversion of GO to CCG in the nanocomposites. The present findings also supported the **FTIR (Fig. 3),** Raman (**Fig. 4**) and XPS **(Fig. 5)** results. It should be pointed out that in ZEG(00), a broad UV peak was also found at ~360 nm which shifted towards blue / red wavelength depending upon ZnO crystallite / particle size (as obtained from XRD (**Fig. 1) /** TEM **(Fig. 2 and Fig. S2**), demonstrated the size effect of semiconductor oxide in the nano regime.[26,57] In addition, the spectral region, 240 to 390 nm could be resolved into three Gaussian fitted components, located at 272 nm, 332 nm and 360 nm in ZEG(10) nanocomposite. The peak at 332 nm could relate to electronic transition in the bulk ZnO (band gap, ~ 3.4 eV).

Room temperature photoluminescence (PL) spectra (at different excitation wavelengths) of the ZEG nanocomposites and the other materials are displayed in **Figure 7** and **Figures S5, S6**. The excitation wavelengths were primarily selected from the absorption spectral (measured by diffused reflectance method, **Fig. 6**) study of the nanocomposites. In this context, initially an excitation wavelength of 360 nm was chosen and observed a strong UV PL emission at 384 nm along with several visible emissions (**Fig. S5(a), electronic supporting information**) for ZEG(00) and ZEG(10) nanocomposites. The peak would correspond[12] to the characteristic UV

emission of ZnO due to band-to-band transition. However, fixing the PL emission at 384 nm, the PLE was also recorded and observed the excitation peaks (**inset, Fig. 7a**) at 224 nm, 240 nm and 340 nm. Hence, an excitation wavelength of 340 nm was further used and recorded PL emissions where several distinct visible emissions (**Fig. 7a**) located at ~385 nm, ~420 nm, ~460 nm, ~485 nm, ~520 nm, ~530 nm, ~570 nm and ~595 nm were observed. It was known that except the UV emission at 385 nm, all the visible emissions could relate to intrinsic / extrinsic surface defects of nano ZnO.[26,57-59] However, many researchers are still doubtful about the origin of the individual visible emissions. It could be noted that the formation and nature of the defects depends upon several parameters[26,58,59] (such as preparative method, doping etc.) through which the concentration[26] of an individual defect could be tailored. In this work, the emission observed at 420 nm could support the presence of zinc interstitial[26] while the 460 nm peak could relate to singly positively charged oxygen vacancy in nano ZnO.[26] The existence of antisite oxygen was also supported from the observation of PL emission at 485 nm.[26] Moreover, a series of green emissions were observed (520 nm, 530 nm and 570 nm) in the PL spectra of the nanocomposites. The green emissions[58,59] would be originating from the different levels of oxygen vacancies existed in the nano semiconductor oxide. It was interesting to note that a new PLE peak was observed at 400 nm (**inset (i)** of **Fig. 7b and Fig. S5(b), (c)** of **electronic supporting information**) in addition to 340 nm when the PL emission was fixed at 595 nm. Hence, the excitation at 400 nm was further used to measure the PL spectra which showed a distinct orange emission at 595 nm along with a broad emission in the spectral range, 520-585 nm (**Fig. 7(b)**). Actually, the broad emission consisted of four Gaussian fitted peaks located at 530 nm, 543 nm, 560 nm and 570 nm (**inset (ii), Fig. 7(b)**). These peaks were believed to be originating from the different energy levels of neutral oxygen vacancies in ZnO.[58,59] However,

the intensity of the orange emission at 595 nm could be influenced on Eu incorporation level in the nanocomposites and the highest intensity of the peak was found in ZEG(10) which is approximately twice than the peak intensity of ZEG(00). The origin of the orange emission would be related to interstitial oxygen in the nano semiconductor oxide.[60] Moreover, a systematic broadening of the peak was observed on increasing Eu incorporation level. This peak broadening could be ascertained from the measurement of FWHM where the ZEG(00) and ZEG(15) showed the lowest (11 nm) and the highest (12.5 nm) values of FWHM, respectively. It should mention that the Eu ions being a rare earth could also able for the characteristic emissions especially due to $^5D_0$—$^7F_0$ transition and ^5D_o—$^7F_1$ transitions.[39] Therefore, the broadening could be explained on the basis of increasing Eu incorporation in the nanocomposites but the highest emission intensity in ZEG(10) could certainly be an enhancement of the surface defect (interstitial oxygen) concentration. As XPS (**Fig. 5**) study already confirmed the formation of Eu^{2+} ions in the nanocomposite, perhaps the Eu^{2+} ions in an optimum concentration might be playing a significant role[39] for the enhancement of the intensity of PL emission at 595 nm. On the other hand, the influence of CCG on the intensity of orange emission was also studied in details (**Fig. S6, electronic supporting information**) and noticed a positive function towards enhancement of the defect concentration in hexagonal ZnO of ZEG(10) nanocomposite. Thus, it could conclude that CCG in combination with Eu could assist to enhance the orange emission at 595 nm.

Specific surface area (SSA) of ZEG nanocomposites measured by multipoint BET nitrogen adsorption isotherm (**Fig. S7 and Table S2, electronic supporting information**) found to change with Eu incorporation level. The highest surface area was measured in ZEG(10) nanocomposite. It could be noted that the BET isotherms of the all samples highlight

(**Fig. S7**) an IUPAC Type IV isotherm[61] from the appearance hysteresis loop found in the relative pressure (p/p_o) range of 0.6–1.0, indicated the presence of mesopore in the nanocomposites. We also confirmed the existence of mesopore from the calculated average pore diameter that was found in the range, 11.9 nm to 34.1 nm (**Table S2, electronic supporting information**).

It could believe that during the synthesis, major portions of zinc acetate (ZA) precursor would form[12,22] ZnO nanoparticles (ZNPs) in the reaction medium and remaining ZA would generate Zn^{2+} ions which would chemisorb[12] on the surface of the ZNPs resulting the formation of ZnO/Zn^{2+} moiety. Simultaneously, the GO converted into the chemically converted graphene (CCG) after an appreciable amount of reaction time (**Figs. S1 and S3, electronic supporting information**) and could interact / form complexes with the inorganic moiety. On the other hand, in europium incorporated nanocomposites, no europium ions were found to enter into the ZnO crystal lattice (which might be due to self-purification process[26] in nano semiconductors) as evidenced from the XRD result (**Fig. 1**). However, these ions could interact / form complexes with the free oxygen functional groups of CCG as confirmed by FTIR (**Fig. 3**), Raman (**Fig. 4**) and XPS (**Fig. 5**) and UV-Vis (**Fig. 6**) studies. However, TEM studies (**Fig. 2**) confirmed the presence of CCG layer onto the surface of ZnO nano crystals. Thus, in the present work, on the basis of our experimental results, a tentative chemical structure of europium incorporated ZEG nanocomposite is given in **Figure 8**.

Due to unique physical and optical properties of ZnO nanoparticles, these could have significant advantages in biomedical applications (e.g. cell imaging and drug delivery)[19,20]. Also, the nanoparticles (NPs) could possess particle size dependent tunable band edge emission[23] in the ultraviolet region. Moreover, these could be capable to generate visible

emissions[26] due to the presence of several intrinsic / extrinsic surface defects. Hence, it would possible to utilize a suitable visible emission towards the application of cell imaging. In this regard, it could no doubt that many studies[24,58] had already been performed on ZnO nanoparticles. In the present work, the PL study already confirmed the existence of an orange emission at 595 nm (λ_{ex} = 400 nm) in the nanocomposites. Moreover, the intensity of the orange emission that was found to be dependent on EUN/ZA molar ratio (R value) where ZEG(10) sample exhibited the highest intensity over the others and proved the necessity of Eu incorporation in an optimum amount in the ZnO graphene nanocomposite to obtain the high intensity of the orange emission. Hence, the ZEG(10) nanocomposite could be expected to have a better cell imaging capability. We have checked the performance of ZEG(10) comparing with ZEG(00) for the human breast cancer cell (MCF7) imaging under confocal laser scanning microscope. The DIC pictures and the fluorescent images were taken (**Fig. 9a**) for a fixed concentration (100 µg/ml) of ZEG nanocomposites. From the images, it was clear that the internalization of the nanomaterials within the living cells happened. A bright cell images were found due to the orange fluorescence of the nanocomposites under the microscope. Anyhow, a relative intensity of the images (**Fig. S8, electronic supporting information**) were calculated using imageJ software and analyzed by one way ANNOVA. It was noted that the highest intensity (**Fig. S8, electronic supporting information**) was found when ZEG(10) nanocomposite was used and in this case, the intensity found more than two times higher (**Fig. S8, electronic supporting information**) compare to ZEG(00) nanocomposite. The intensity of the orange fluorescence also corroborated the PL results (**Fig. 7b**). Hence, the orange emission of ZEG(10) nanocomposite could be useful for the study of cell imaging.

ZnO is generally biocompatible and cost effective, but nano ZnO has been classified as "extremely toxic" in the environment.[35] The extreme toxicity of nano ZnO could generally be mitigated to make biocompatible through coating on the surface of the nano semiconductor oxide by graphene derivatives. It could be noted that graphene possesses large surface area, chemical purity and possibility of easy functionalization with suitable semiconductor[20] or suitable organic molecule.[6,7] Therefore, graphene based ZnO nanocomposite could be used as an alternative of organic dyes[62] for the cell imaging purpose. However, for further improvement of the property, proper modification of nano matrix would be necessary and incorporation of Eu in an optimum amount would be beneficial in this respect. In the present work, a relatively better cell imaging performance (**Fig. 9a**) was found in ZEG(10). It was known that the toxic effect of nanocomposites on biological cells (known as cytotoxicity) could depend upon their several characteristics.[63] It had already been demonstrated that nano ZnO exhibited toxic effect in mammalian cells.[32] This could be due to particle dissolution in the tissue culture medium and intracellularly resulting from Zn^{2+} shedding. It was also reported that the doping[35] with Fe could be an effective way to reduce particle dissolution of nano ZnO for the concern application. Thus, the change of particle matrix as well as the rate of particle dissolution could be slowed down by Fe doping. On the other hand, graphene based semiconductors (e.g. ZnS, CdSe) NPs[20] reported to have an effective cell imaging as well as high cell viability. In this work, we measured the cytotoxicity in terms of measuring the cell viability of human breast cancer cells (MCF7) with ZEG nanocomposites (**Fig. 9b**). An approximately 74% viable cells were observed in ZEG(10) for 30 μg/ml ZEG nanocomposite concentration in 24 h duration. However, the low cell viability was observed for the ZEG(00) nanocomposite where no Eu was incorporated. Moreover, the cell viability remained nearly same in ZEG(15) nanocomposite

compare to ZEG(10). This would be arising from the same I_D/I_G value (**Fig. 4, Table S1 of electronic supporting information**), generating due to exfoliation[31] of graphene layers through interaction / complexation between free organic functional groups of CCG and the inorganic moieties present in the nanocomposite as already observed from Raman spectral study. Hence, the observation clearly indicates that an optimum concentration of Eu incorporation in the nanocomposite was necessary to obtain better cell viability. Usually, the better cell viability and cell imaging capability as well as relatively large surface area could make the materials an effective carrier for drug delivery.[64] In this respect, the Eu incorporated nanocomposites ($R \geq 0.10$) could find application in drug delivery.

Conclusion

Europium incorporated ZnO-chemically converted graphene (CCG) nanocomposites were synthesized from the precursors of varying europium nitrate to zinc acetate molar ratio (R = 0.00, 0.05, 0.10 and 0.15) in a fixed content of graphene oxide adopting a low temperature (95^oC) solvothermal process. The change of crystallite / particle size of hexagonal ZnO found dependent on Eu incorporation level (R value). In the nanocomposites, an evidence of chemical interaction / complexation with the oxygen functionalities of CCG and inorganic moieties (ZnO/Zn^{2+} and Eu ions) was found. Although, the nanocomposite, ZEG(10) (R = 0.10) showed highest specific surface area but all the samples possessed meso pores. In addition to an UV emission, an orange emission appeared at 595 nm along with other visible emissions were observed from photoluminescence spectra of the nanocomposites. However, the intensity of the orange emission found maximum in the nanocomposite, ZEG(10). Under confocal laser scanning microscope, a bright orange fluorescence images of human breast cancer cells (MCF7)

with the ZEG(10) nanocomposite was found indicating internalization of the nanomaterials within the cells. The nanocomposite also exhibited comparatively low *in vitro* cytotoxicity on the cells. The ZEG(10) nanocomposite would be employed for cancer cell targetted optical imaging and drug delivery.

Acknowledgements

Authors are grateful to the Director, CSIR-CGCRI, Kolkata for his kind support, encouragement and permission to publish this work. The authors, SB, MG and MP thankfully acknowledge CSIR and UGC, Govt. of India for providing their Ph.D. research fellowships under NET Fellowship scheme. The authors also acknowledge the help rendered by Nanostructured Materials Division and Electron Microscopy Section for Raman and microstructural characterizations respectively. The work has been done as an associated research work of 12th Five Year Plan project of CSIR (No. ESC0202).

References

1 S. Stankovich, D. A. Dikin, G. H. B. Dommett, K. M. Kohlhaas, E. J. Zimney, E. A. Stach, R. D. Piner, S. B. T. Nguyen and R. S. Ruoff, *Nature*, 2006, **442**, 282-286.

2 X. Huang, X. Qi, F. Boey and H. Zhang, *Chem. Soc. Rev*., 2012, **41**, 666-686.

3 F. Schedin, A. K. Geim, S. V. Morozov, E. W. Hill, P. Blake, M. I. Katsnelson and K. S. Novoselov, *Nat. Mater*., 2007, **6**, 652-655.

4 S. Park and R. S. Ruoff, *Nat. Nanotechnol*., 2009, **4**, 217-224.

5 F. Liu, C. W. Lee and J. S. Im, *J. Nanomater*., 2013, **2013** (11 pages).

6 Q. Wu, Y. Xu, Z. Yao, A. Liu, and G. Shi, *ACS Nano*, 2010, **4**, 1963–1970.

7 A. Kundu, R. K. Layek, A. Kuila, and A. K. Nandi, *ACS Appl. Mater. Interfaces*, 2012, **4**, 5576−5582.

8 R. Pasricha, S. Gupta, and A. K. Srivastava, *Small*, 2009, **5**, 2253–2259.

9 J. Li, C.-y. Liu and Y. Liu, *J. Mater. Chem*., 2012, **22**, 8426–8430.

10 O. Ü. Aktürk and M. Tomak, *Phys. Rev. B*, 2009, **80**, 085417 (6 pages).

11 B. K. Gupta, P. Thanikaivelan, T. N. Narayanan, L. Song, W. Gao, T. Hayashi, A. L. M. Reddy, A. Saha, V. Shanker, M. Endo, A. A. Marti and P. M. Ajayan, *Nano Lett*., 2011, **11**, 5227-5233.

12 D. I. Son, B. W. Kwon, D. H. Park, W.-S. Seo, Y. Yi, B. Angadi, C.-L. Lee and W. K. Choi, *Nat. Nanotechol*., 2012, **7**, 465-471.

13 D. Wang, D. Choi, J. Li, Z. Yang, Z. Nie, R. Kou, D. Hu, C. Wang, L. V. Saraf, J. Zhang, I. A. Aksay, and J. Liu, *ACS Nano*, 2009, **3**, 907–914.

14 G. Zhou, D.-W. Wang, F. Li, L. Zhang, N. Li, Z.-S. Wu, L. Wen, G. Q. (Max) Lu and H.-M. Cheng, *Chem. Mater*., 2010, **22**, 5306–5313.

15 L. Peng, X. Peng, B. Liu, C. Wu, Y. Xie, and G. Yu, *Nano Lett*., 2013, **13**, 2151−2157.

16 H. Kim, S. -W. Kim, Y. -U. Park, H. Gwon, D.- H. Seo, Y. Kim, and K. Kang, *Nano Res*., 2010, **3**, 813–821.

17 Z. -S. Wu, W. Ren, L. Wen, L. Gao, J. Zhao, Z. Chen, G. Zhou, F. Li, and H.-M. Cheng, *ACS Nano*, 2010, **4**, 3187–3194.

18 F. Bonaccorso, Z. Sun, T. Hasan and A. C. Ferrari, *Nat. Photon*., 2010, **4**, 611-622.

19 C. Chellaram, A. A. John, M. M. Praveen, R. Sivakumar, N. Kumar and H. Archana, *Int. Res. Pharm. Sci*., 2013, **4**, 366-370.

20 S.-H. Hu, Y.-W. Chen, W.-T. Hung, I.-W.Chen and S.-Y. Chen, *Adv. Mater.*, 2012, **24**, 1748-1754.

21 Q. Zhang, C. Tian, A. Wu, T. Tan, L. Sun, L. Wang and H. Fu, *J. Mater. Chem.*, 2012, **22**, 11778–11784.

22 D. I. Son, B. W. Kwon, J. D. Yang, D. H. Park, W. S. Seo, H. Lee, Y. Yi, C. L. Lee and W. K. Choi, *Nano Res.*, 2012, **5**, 747–761.

23 O. Lupan, T. Pauporte, T. L. Bahers, B. Viana and I Ciofini, *Adv. Funct. Mater.*, 2011, **21**, 3564–3572.

24 H.-M. Xiong, Y. Xu, Q.-G. Ren and Y.-Y. Xia, *J. Am. Chem. Soc.*, 2008, **130**, 7522-7523.

25 Z. Zhan, L. Zheng, Y. Pan, G. Sun and L. Li, *J. Mater. Chem.*, 2012, **22**, 2589–2595.

26 M. Pal, S. Bera, S. Sarkar and S. Jana, *RSC Adv.*, 2014, **4**, 11552-11563.

27 P. Jakes and E. Erdem, *physica status solidi rrl.*, 2011, **5**, 56-58

28 H. Kaftelen, K. Ocakoglu, R. Thomann, S. Tu, S. Weber and E. Erdem, *Phys. Rev. B,* 2012, **86**, 014113 (9 pages)

29 M. Açıkgöz, M. D. Drahus, A. Ozarowski, J. v. Tol, S. Weber and E. Erdem, *J. Phys.: Condens. Matter.*, 2014, **26**, 155803 (9 pages)

30 S. Gurunathan, J. W. Han, V. Eppakayala, A. A. Dayem, D.-N. Kwon and J.-H. Kim, *Nanoscale Res. Lett*., 2013, **8**, 393 (13 pages).

31 H. Chen, M. B. Muller, K. J. Gilmore, G. G. Wallace and D. Li, *Adv. Mater.*, 2008, **20**, 3557-3561.

32 X. Dou, *Thermodyn. Catal.*, 2012, **3** (2 pages).

33 K. Spyrou and P. Rudolf, *An introduction to graphene*, ed., V. Georgakilas, *in*, *Functionalization of graphene, Wiley-VCH, Weinheim*, 2014.

34 M. C. Duch, G. R. S. Budinger, Y. T. Liang, S. Soberanes, D. Urich, S. E. Chiarella, L. A. Campochiaro, A. Gonzalez, N. S. Chandel, M. C. Hersam and G. M. Mutlu, *Nano Lett*., 2011, **11**, 5201-5207.

35 T. Xia, Y. Zhao, T. Sager, S. George, S. Pokhrel, N. Li, D. Schoenfeld, H. Meng, S. Lin, X. Wang, M. Wang, Z. Ji, J. I. Zink, L. Madler, V. Castranova, S. Lin, and A. E. Nel, *ACS Nano*, 2011, **5**, 1223–1235.

36 D. Wang, H. Gao, E. Roze, K. Qu, W. Liu, Y. Shao, S. Xin and Y. Wang, *J. Mater. Chem. C*, 2013, **1**, 5772–5778.

37 Y. Sun, Q. Wang, C. Chen, X. Tan and X. Wang, *Environ. Sci. Technol*., 2012, **46**, 6020-6027.

38 Y.-P. Du, Y.-W. Zhang, L.-D. Sun and C.-H. Yan, *J. Phys. Chem. C*, 2008, **112**, 12234-12241.

39 X. Zeng, J. Yuan, Z. Wang and L. Zhang, *Adv. Mater*., 2007, **19**, 4510–4514.

40 R. Chen, Y. Q. Shen, F. Xiano, B. Liu, G.G. Gurzadyan, Z. L. Dong, X. W. Sun and H. D. Sun, *J. Phys. Chem. C*, 2010, **114**, 18081-18084.

41 L.-W. Sun, H.-Q. Shi, W.-N. Li, H.-M. Xiao, S.-Y. Fu, X. -Z. Cao and Z.-X. Li, *J. Mater. Chem*., 2012, **22**, 8221–8227.

42 B. Li and H. Cao, *J. Mater. Chem*., 2011, **21**, 3346-3349.

43 X. Liu, L. Pan, T. Lv, T. Lu, G. Zhu, Z. Sun and C. Sun, *Catal. Sci. Technol*., 2011, **1**, 1189-1193.

44 Q. Min, X. Zhang, H. Zhang, F. Zhou and J.-J. Zhu, *Chem. Commun.*, 2011, **47**, 11709–11711.

45 H. Hayashi, I. V. Lightcap, M. Tsujimoto, M. Takano, T. Umeyama, P. V. Kamat and H. Imahori, *J. Am. Chem. Soc.*, 2011, **133**, 7684–7687.

46 X. Xia, Q. Hao, W. Lei, W. Wang, D. Sun and X. Wang, *J. Mater. Chem.*, 2012, **22**, 16844–16850.

47 R. Kou, Y. Shao, D. Mei, Z. Nie, D. Wang, C. Wang, V. V. Viswanathan, S. Park, I. A. Aksay, Y. Lin, Y. Wang and J. Liu, *J. Am. Chem. Soc.*, 2011, **133**, 2541–2547.

48 A. Ganguly, S. Sharma, P. Papakonstantinou and J. Hamilton, *J. Phys. Chem. C*, 2011, **115**, 17009–17019.

49 J. Liang, W. Wei, D. Zhong, Q. Yang, L. Li and L. Guo, *ACS Appl. Mater. Interfaces*, 2012, **4**, 454−459.

50 X. Yu, X. Xu, T. Jiang, H. Yu, P. Yang, Q. Jiao, J. Qiu, *Mater. Chem. Phys.*, 2013, **139,** 314-318.

51 Y. Yang, L. Ren, C. Zhang, S. Huang and T. Liu, *ACS Appl. Mater. Interfaces*, 2011, **3**, 2779-2785.

52 B.-L. An, M.-L. Gong, M.-X. Li, J.-M. Zhang, Z.-X. Cheng, *J. Fluoresc.*, 2005, **15**, 613-617.

53 L.-G. Tang, D. N.-S. Hon, *J. Appl. Polym. Sci.*, 2001, **79**, 1476-1485.

54 S. Bera, M. Pal, S. Sarkar, S. Jana, *Appl. Surf. Sci.*, 2013, **273**, 39–48.

55 F. Mercier, C. Alliot, L. Bion, N. Thromat and P. Toulhoat, *J. Electron Spectrosc. Relat. Phenom.*, 2006, **150**, 21-26.

56 X. Lv and J. Weng, *Sci. Rep.*, 2013, **3**, 3285 (10 pages).

57 S. Jana, A.S. Vuk, A. Mallick, B. Orel, P.K. Biswas, *Mater. Res. Bull.*, 2011, **46**, 2392–2397.

58 X. Tang, E. S. G. Choo, L. Lee, J. ding and J. Xue, C*hem. Mater.*, 2010, **22**, 3383–3388.

59 H. Zeng, G. Duan, Y. Li, S. Yang, X. Xu and W. Cai, *Adv. Func. Mater.*, 2010, **20**, 561-572.

60 L. E. Greene, M. Law, J. Goldberger, F. Kim, J. C. Johnson, Y. Zhang, R. J. Saykally and P. Yang, *Angew. Chem. Int. Ed*., 2003, **42**, 3031–3034.

61 N. Das, S. Jana and P. K. Biswas, *Sci. Adv. Mater.*, 2014, **6**, 1-11.

62 U. Resch-Genger, M. Grabolle, S. Cavaliere-Jaricot, R. Nitschke and T. Nann, *Nat. Methods*, 2008, **5**, 763-775.

63 Y.-N. Chang, M. Zhang, L. Xia, J. Zhang and G. Xing, *Materials*, 2012, **5**, 2850-2871.

64 H. Hong, J. Shi, Y. Yang, Y. Zhang, J. W. Engle, R. J. Nickles, X. Wang and W. Cai, *Nano Lett*., 2011, **11**, 3744-3750.

Figure captions

Fig. 1: XRD reflections of ZEG nanocomposites and as-synthesized graphene oxide. Inset shows the change of crystallite size on increasing Eu incorporation level in the precursors.

Fig. 2: TEM images (a), (c) and (e) of ZEG(00), ZEG(10) and ZEG(15) respectively. Respective histograms show particle size distributions of nanocomposites (insets of (c) and inset (i) of (e)). HRTEM images of ZEG(00), ZEG(10) and ZEG(15) are shown in (b), (d) and (f), respectively. TEM-EDS of ZEG(10) and ZEG(15) are given in the insets of (d) and (f) respectively. Inset (ii) of (e) shows the FFT from the HRTEM (f). HRTEM (f) was taken from the selected (image marked by red square) as shown in (e).

Fig. 3: FTIR spectra of different nanocomposites along with as-synthesized graphene oxide.

Fig. 4: Raman spectra of ZEG nanocomposites. Individual I_D/I_G value is also embedded in the figure.

Fig. 5: XPS data of ZEG(10) nanocomposite: Binding energy spectra of (a) C1s and (b) O1s along with their Gaussian-fitted components; (c) typical XPS data for the binding energy spectrum of $Zn2p_{3/2}$ and $Zn2p_{1/2}$ core levels; (d) shows the binding energy spectrum of Eu 3d core levels.

Fig. 6: Absorption spectra of ZEG nanocomposites along with as-synthesized graphene oxide. Inset (i) shows the enlarged spectrum (as marked) of graphene oxide while inset (ii) indicates the Gaussian-fitted components of the spectrum in wavelength range, 240-430 nm for ZEG(10).

Fig. 7: (a) Photoluminescence emission spectra (λ_{ex} = 340 nm) of ZEG nanocomposites (inset shows the photoluminescence excitation spectrum, fixing the emission at 384 nm). (b) Photoluminescence emission spectra (λ_{ex} = 400 nm) of ZEG nanocomposites (inset (i) shows the photoluminescence excitation spectrum, fixing the emission at 595 nm while inset (ii)

describes the Gaussian-fitted components of the marked portion in the wavelength range, 520-585 nm for ZEG(10).

Fig. 8: A scheme illustrating the synthesis of graphene oxide from graphite powder as well as formation of Eu incorporated ZnO-chemically converted graphene. A possible chemical structure of Eu incorporated ZnO-graphene nanocomposite is also displayed in the scheme.

Fig. 9: (a) DIC pictures (i, iii, v) and fluorescence images (ii, iv, vi) of the MCF7 breast cancer cells under confocal laser scanning microscope; (b) Cell viability results from a MTT assay with ZEG nanocomposites of different concentrations. The error bars represent ±SD ($P<0.05$).

Figures

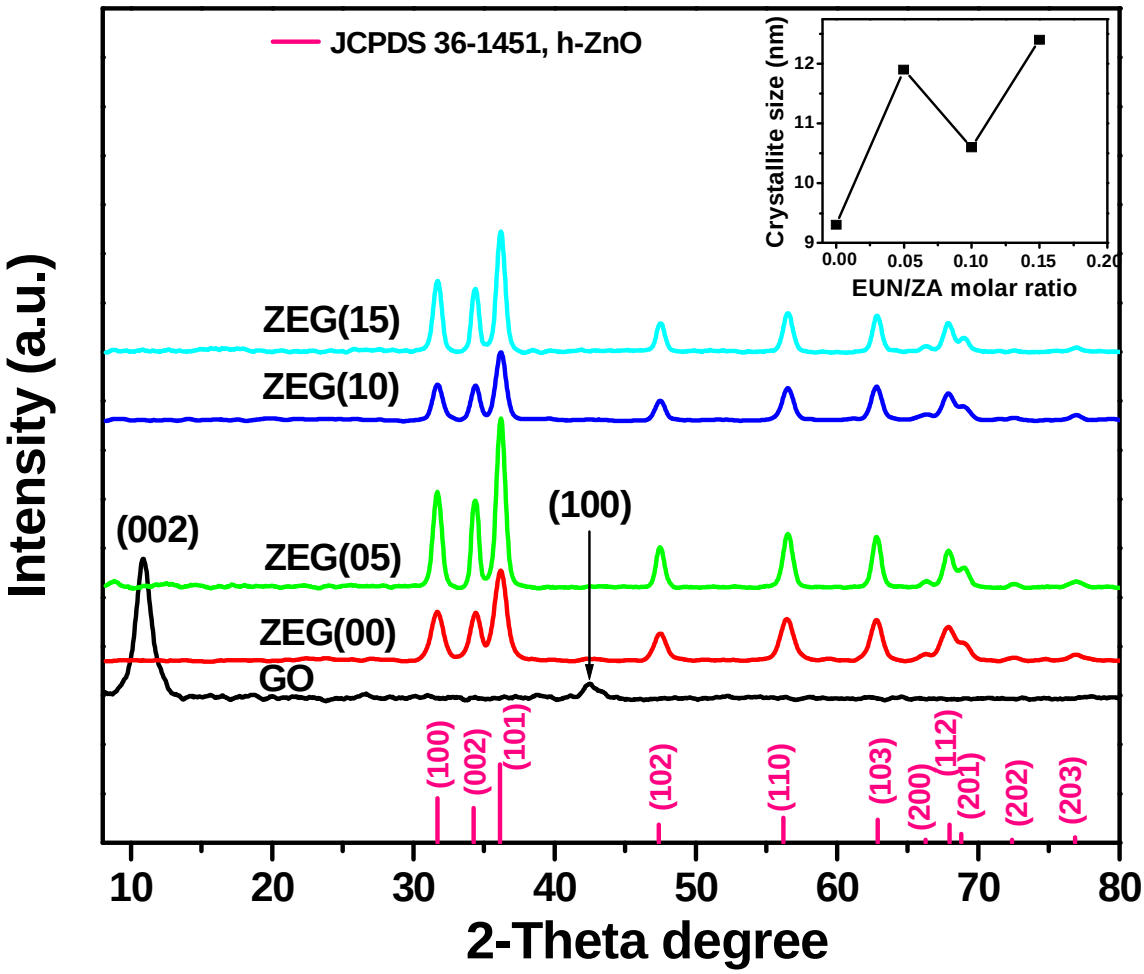

Fig: 1:

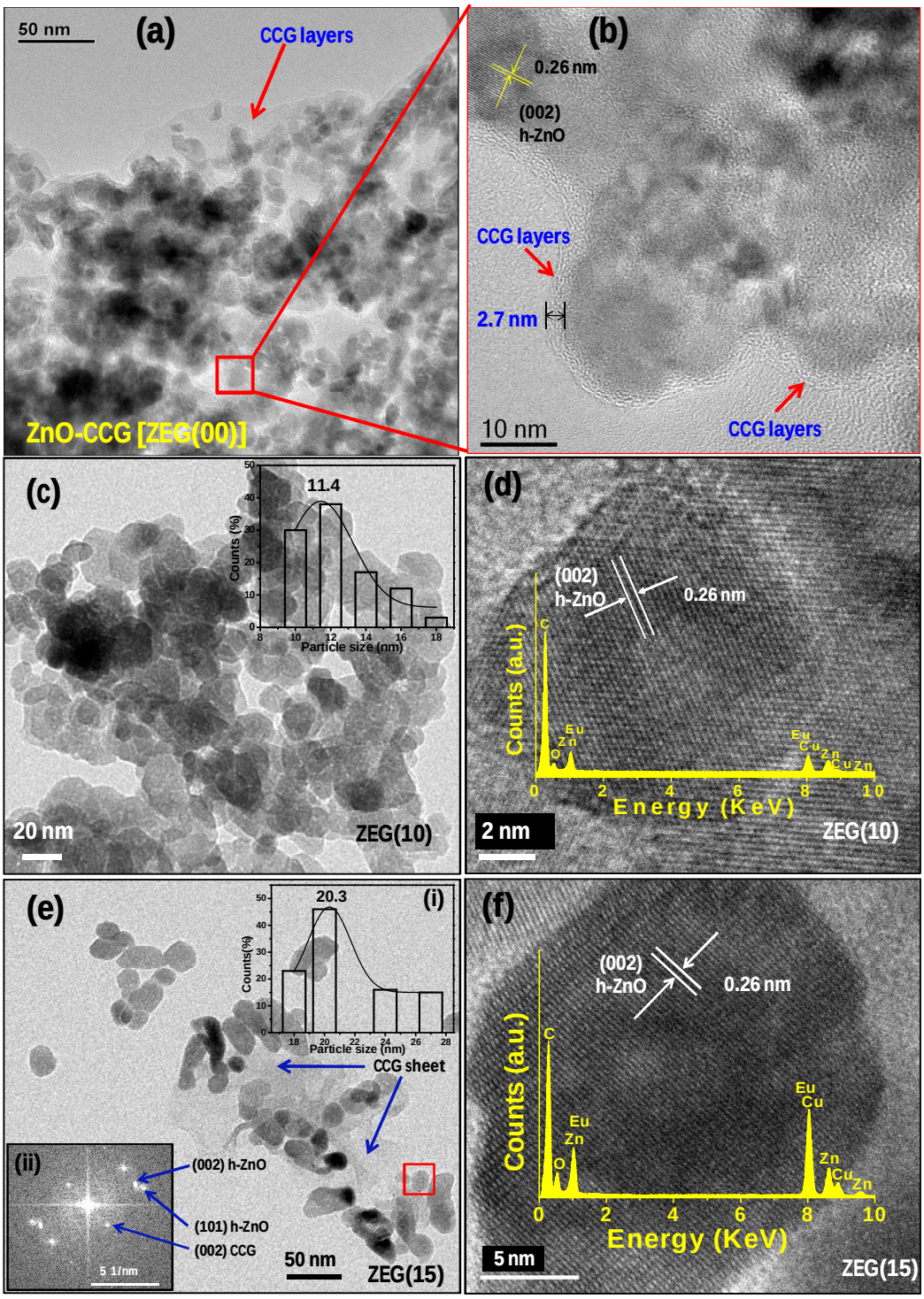

Fig: 2:

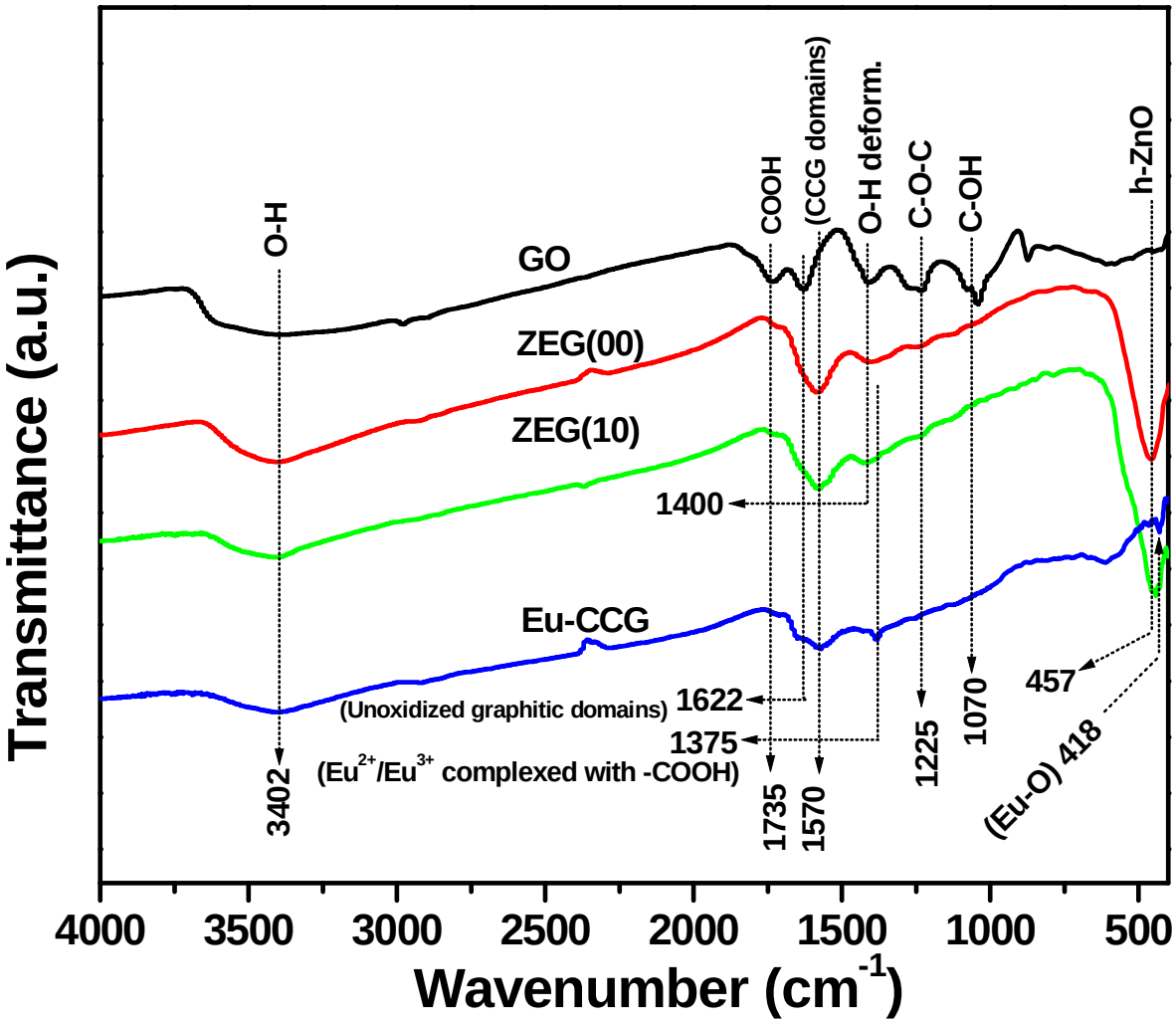

Fig. 3:

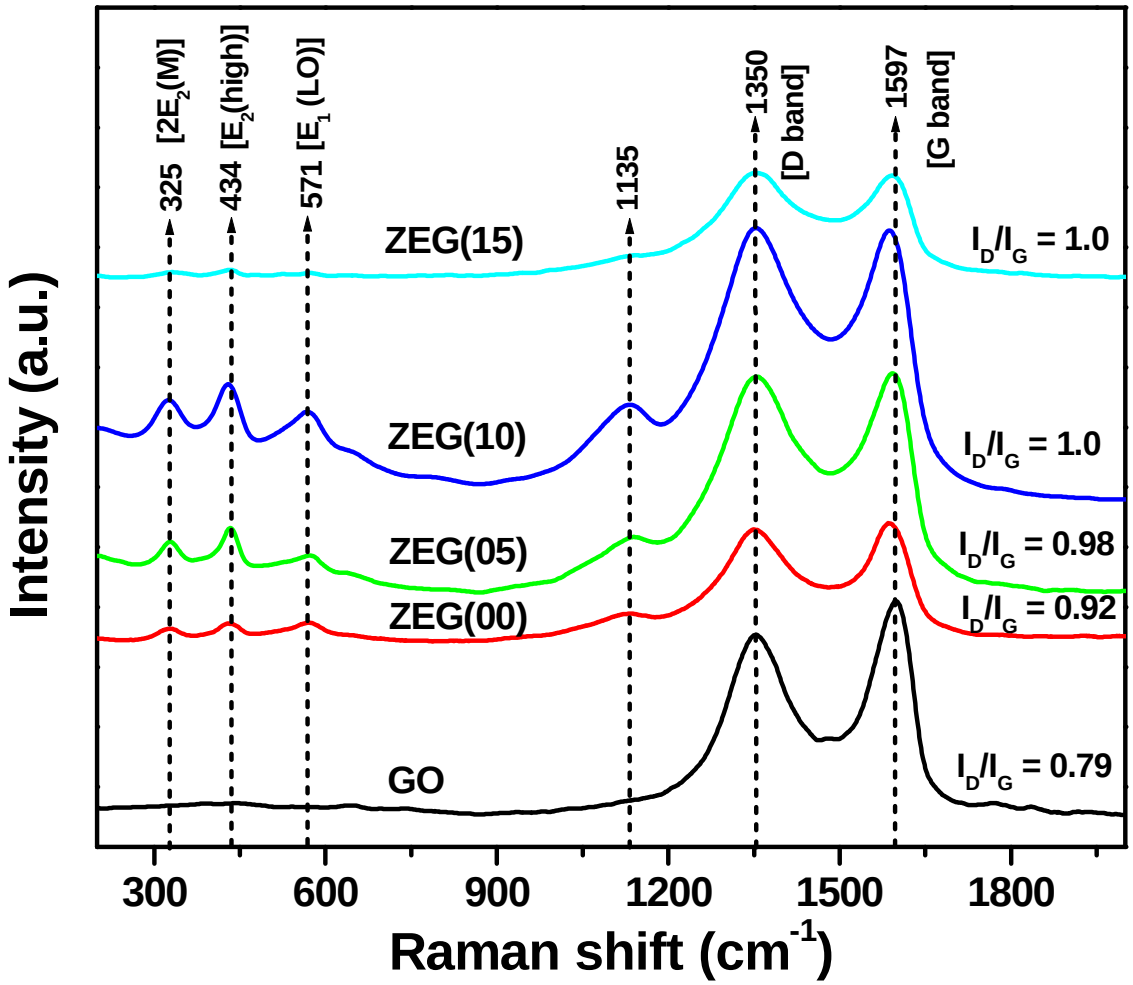

Fig. 4:

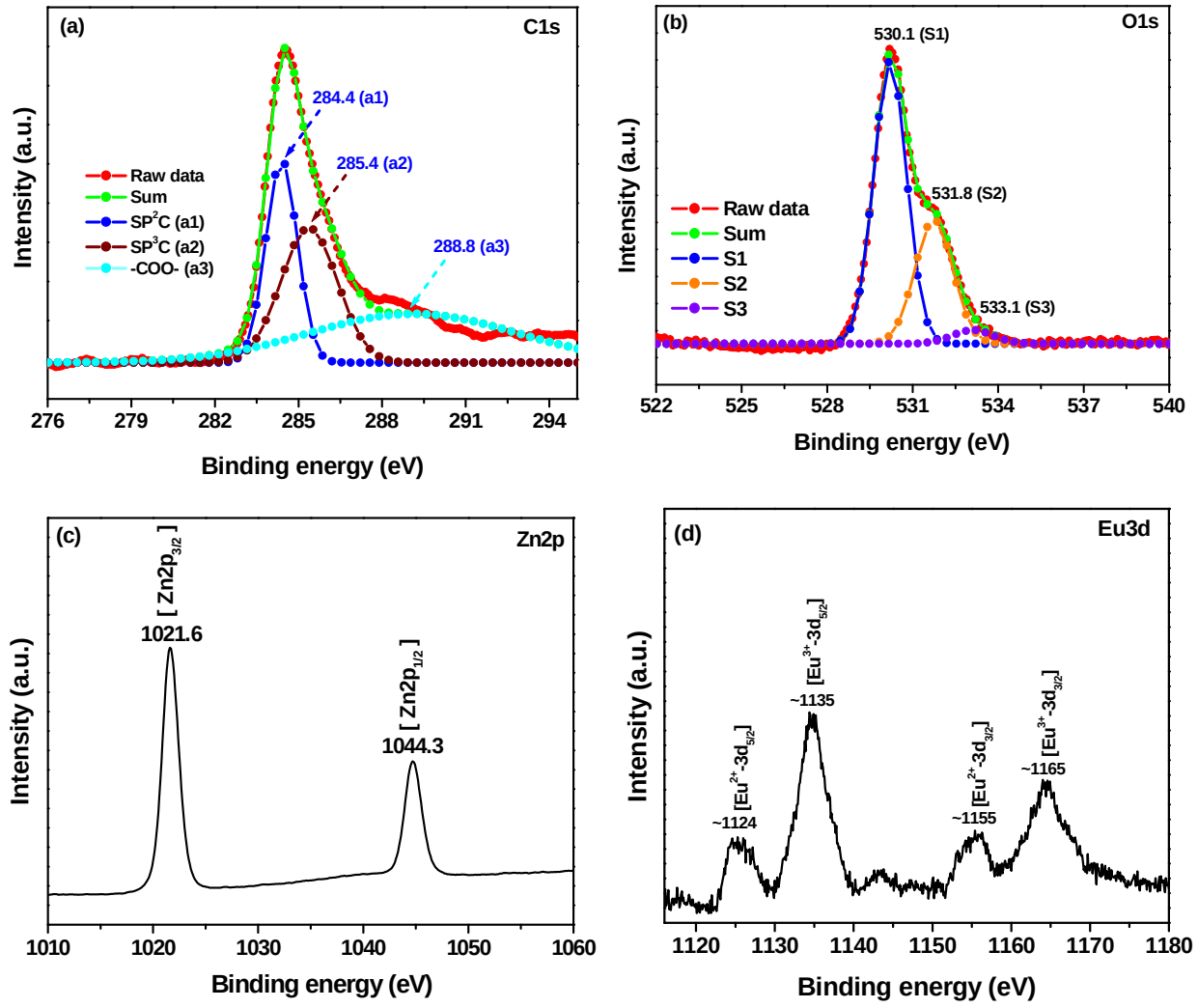

Fig. 5:

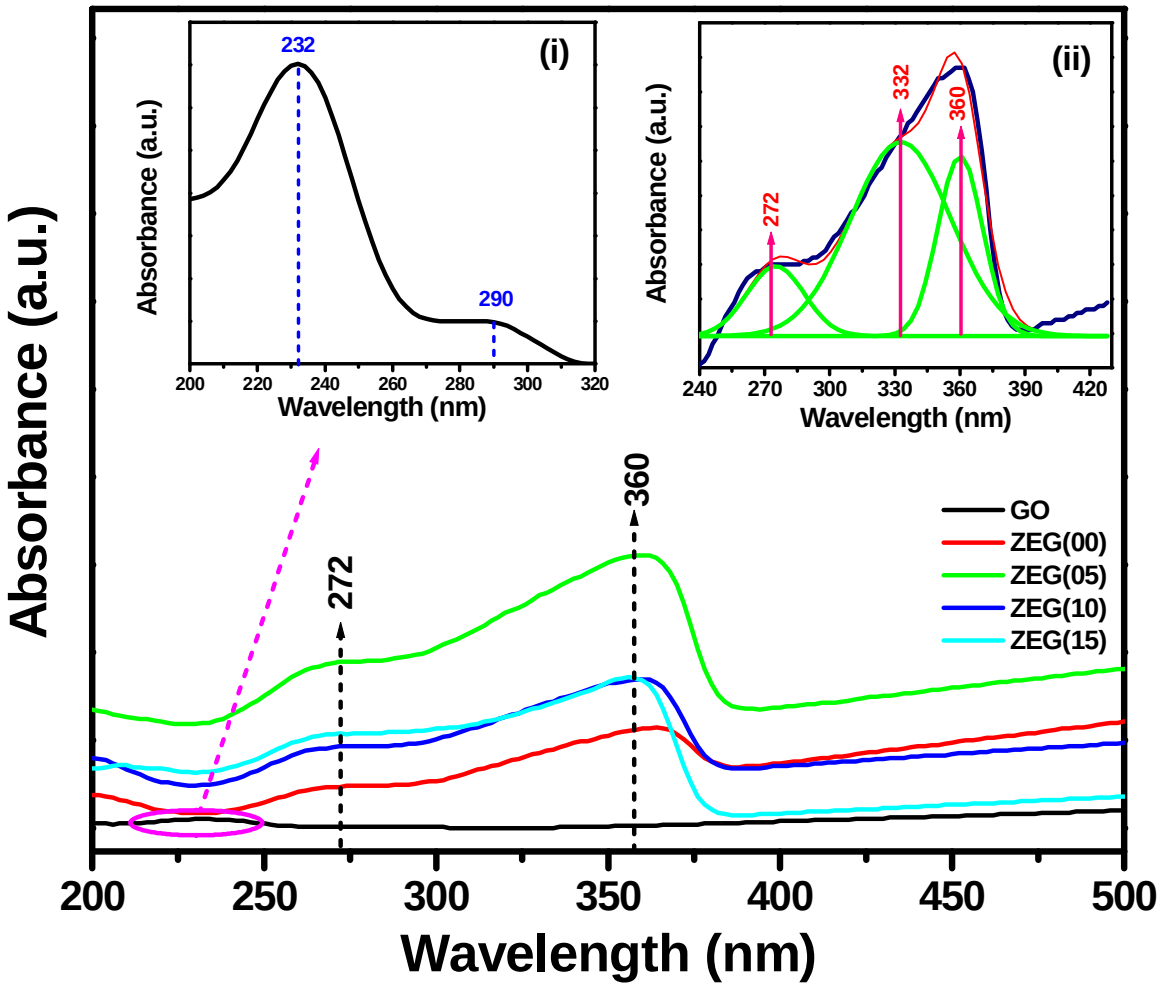

Fig. 6:

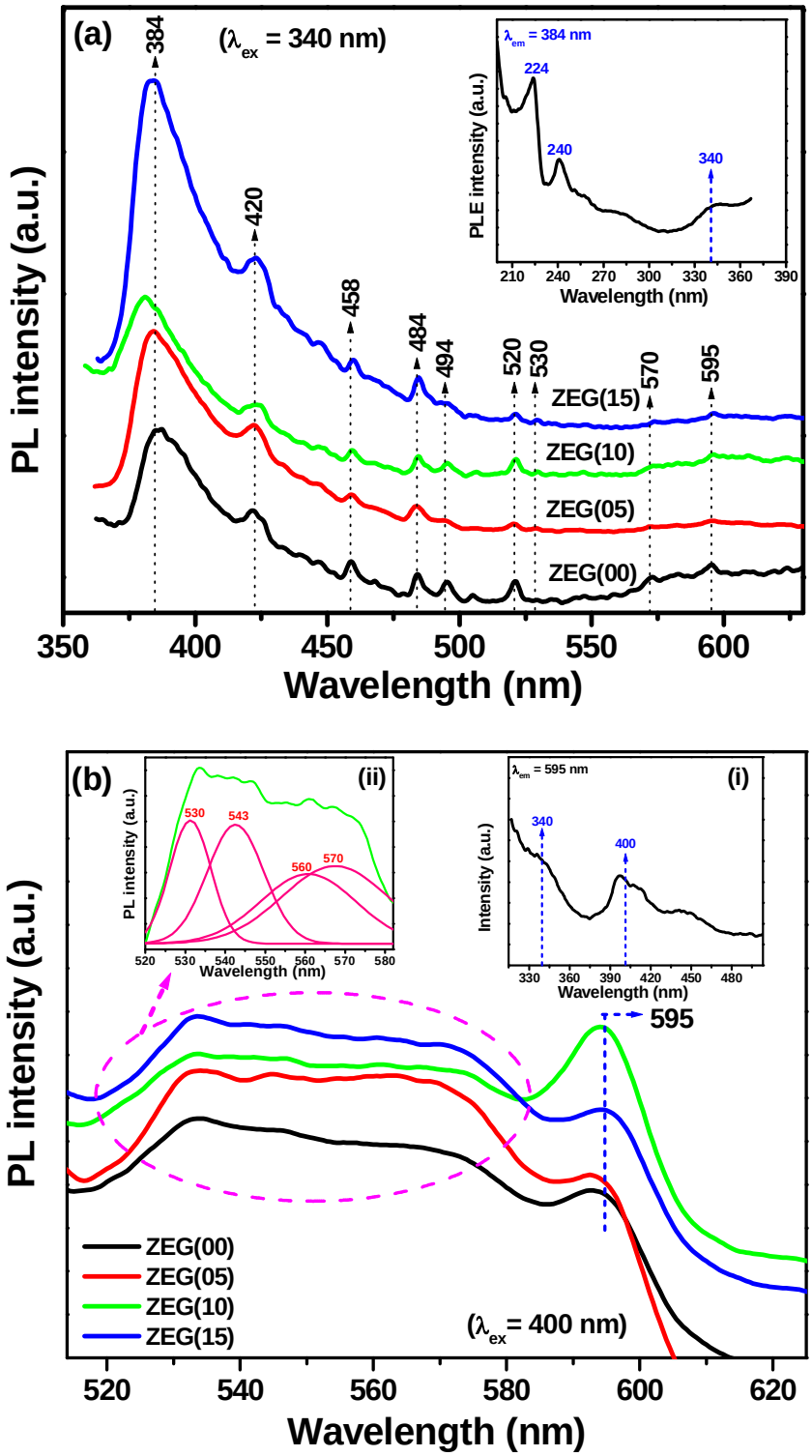

Fig. 7:

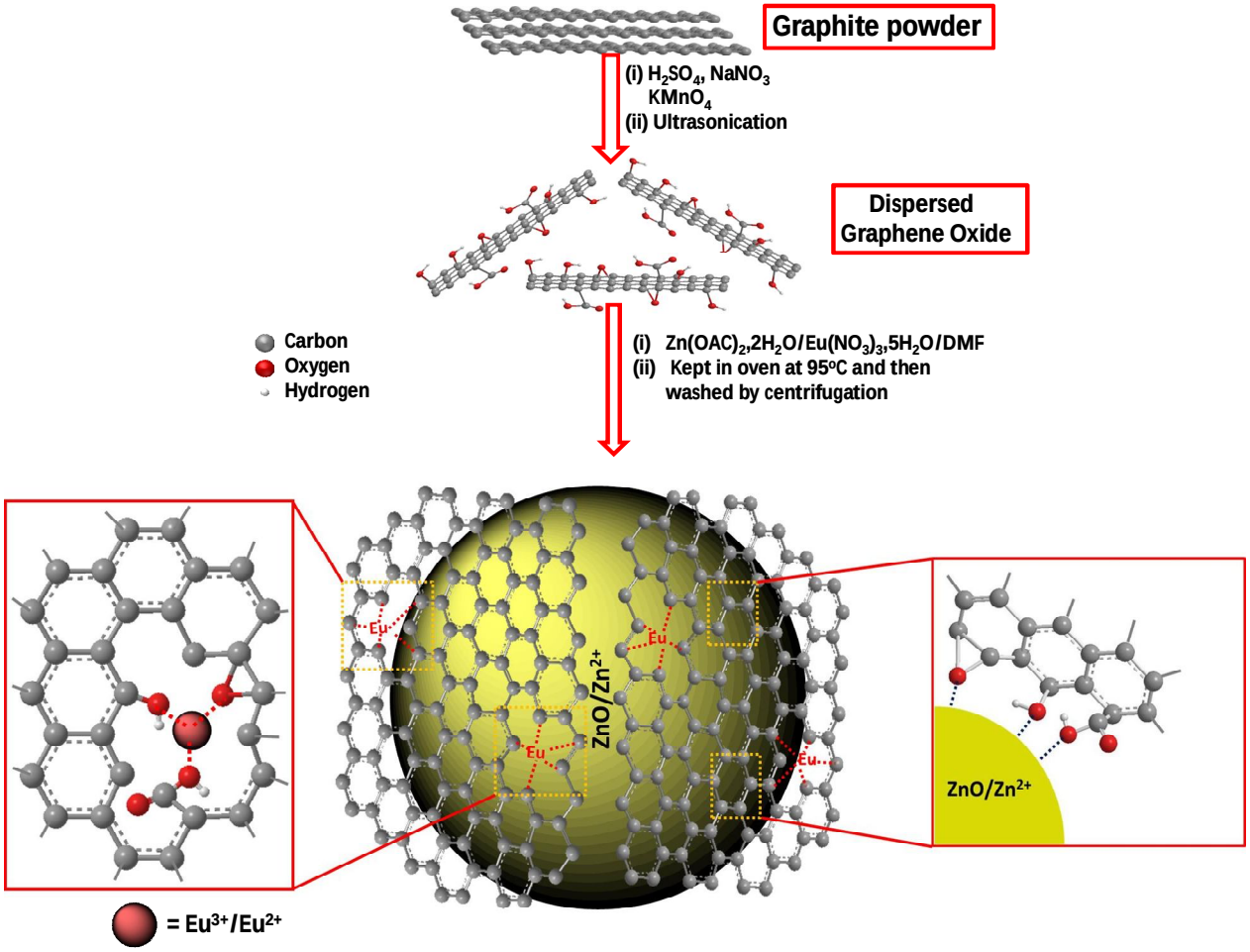

Fig. 8:

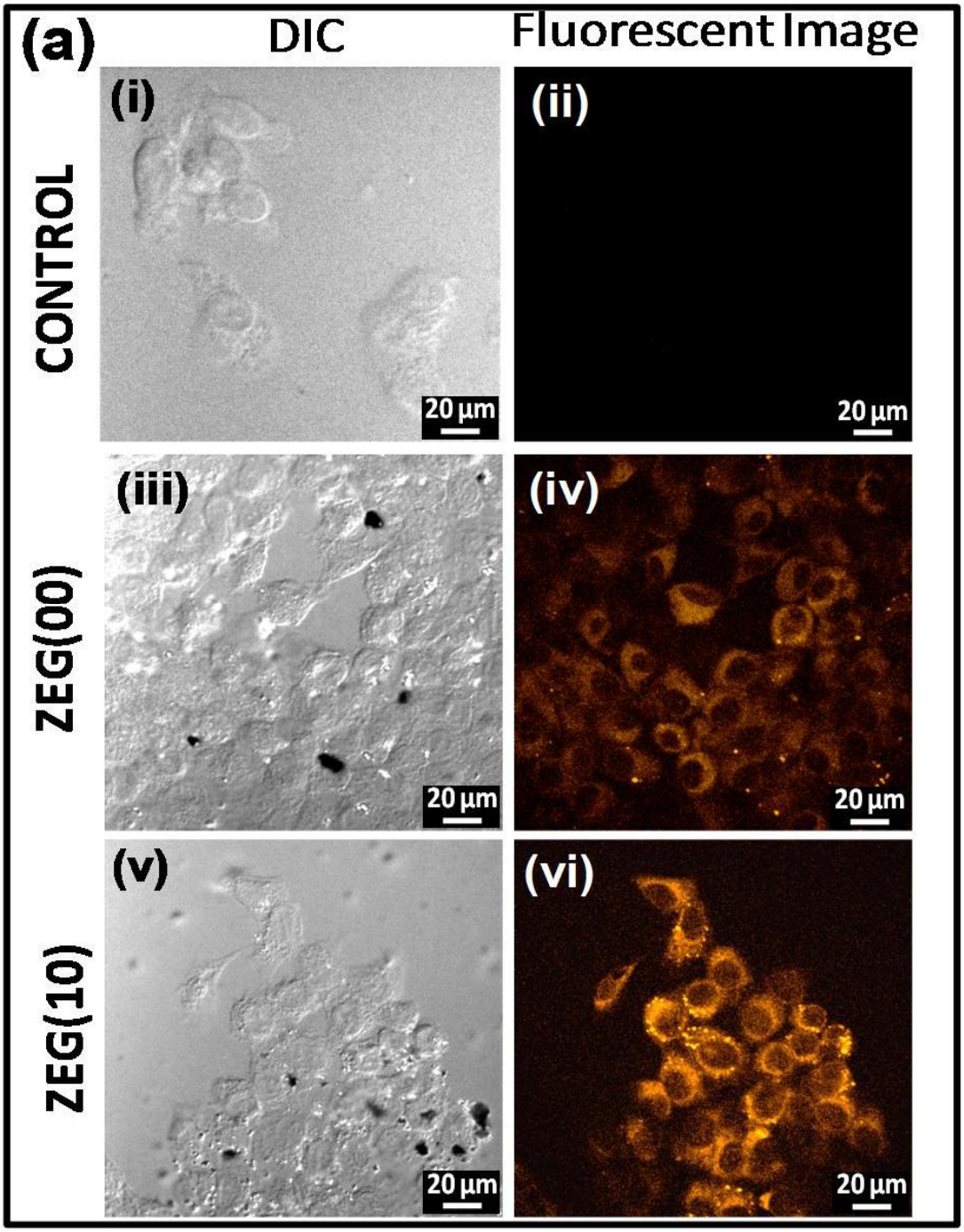

Fig. 9(a):

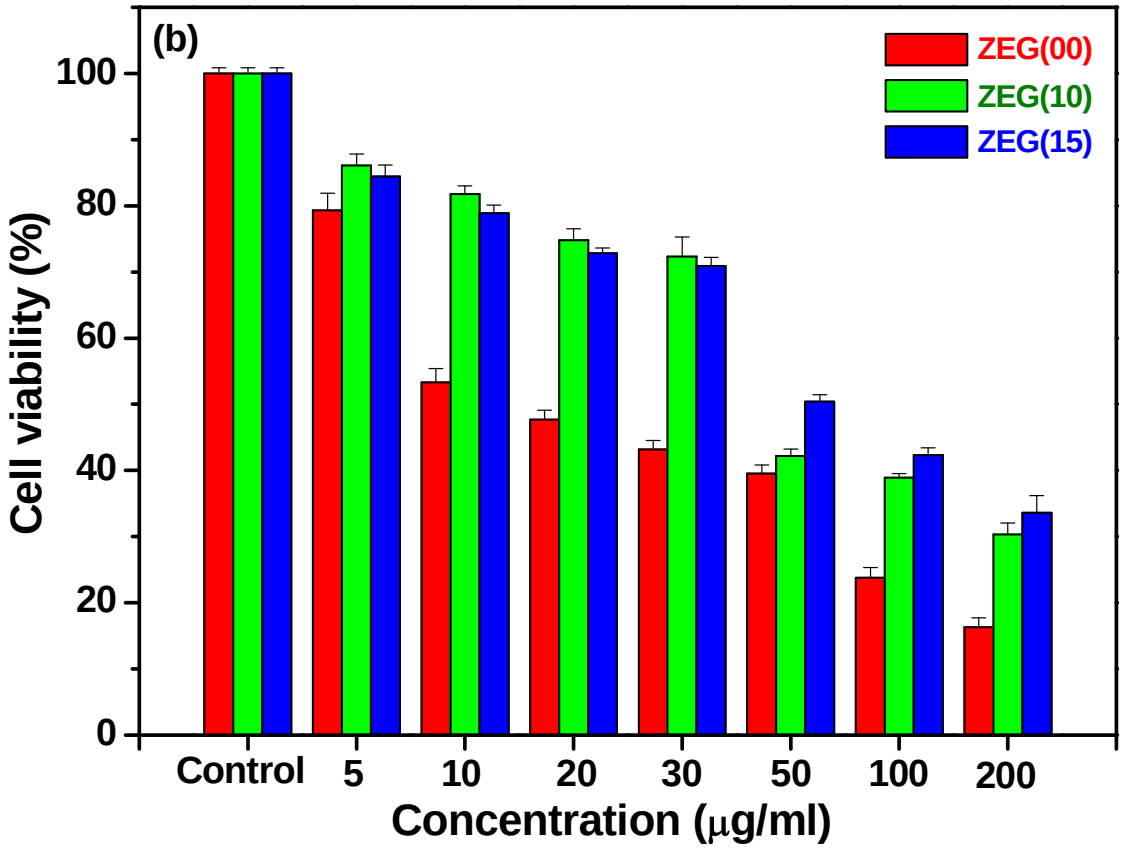

Fig. 9(b):